Journal of Materials Chemistry A

ROYAL SOCIETY OF CHEMISTRY

PAPER

View Article Online
View Journal | View Issue

Published on 18 December 2019. Downloaded by Chinese University of Hong Kong on 10/25/2021 4:50:13 PM.

Check for updates

Cite this: J. Mater. Chem. A, 2020, 8, 1724

A highly stretchable and conductive composite based on an emulsion-templated silver nanowire aerogel†

Zhilin Tian,[ab] Yu Zhao,[c] Shaogang Wang,[d] Guodong Zhou,[b] Ni Zhao *[b] and Ching-Ping Wong *[be]

Received 11th October 2019
Accepted 17th December 2019

DOI: 10.1039/c9ta11225a

rsc.li/materials-a

Stretchable and conductive composites are an important component of flexible electronics. However, it still remains a challenge to achieve high stretchability and high conductivity simultaneously in the composites to ensure high reliability in use. In this work, this issue is addressed by developing an emulsion-template method to fabricate a porous silver nanowire (Ag NW)-based aerogel. The aerogel displays an isotropic and hierarchical microstructure with good uniformity and process controllability. To make the aerogel stretchable, the open cells in the aerogel are infiltrated with an elastomer. The obtained composite exhibits high conductivity (65.7 S cm^{-1}) and good stretchability (130% strain) at a remarkably low density (50 mg cm^{-3}) of Ag NWs, which is enabled by the formation of a three-dimensional conductive and flexible network. The study suggests that the emulsion-templated Ag NW aerogel could be a good candidate for the conductive scaffold of highly stretchable conductors.

Introduction

Flexible and soft electronic devices have seen a rapid development recently because of their great application potential in health monitoring, motion detection, and human–machine interactions.[1] As compared to traditional electronics, flexible devices have lighter weight and can perform under various deformations, thus enabling unconventional functionalities.[2–4] In general, the deformation of the human body can be divided into three regimes (Fig. 1a), small-scale (*e.g.*, skin pulses or facial expressions, <5%); middle-scale (*e.g.*, finger or wrist motions, 5–50%), and large-scale (*e.g.*, joint movements, 50–100%).[1] To accommodate all these types of deformation while minimizing the strains in the active electronic components such as microprocessors, light-emitting diodes, and sensors, one has to use highly stretchable conductors as the interconnects between the electronic components to make the entire system flexible and stretchable.

A key requirement of stretchable conductors is that they should maintain a high conductivity under a large variation of dimensions. There has been great effort devoted to developing materials with high stretchability and conductivity. A commonly used approach is embedding microscale or nanoscale conductive fillers into an elastomeric matrix to form a stretchable conductive composite.[5,6] When reaching a critical concentration, the conductive fillers, such as carbon-based nanomaterials (carbon nanotubes and graphene),[7–10] metal nanowires and liquid metals,[11–14] can form conductive pathways for charge transport while the elastomer, such as polyurethane (PU), polydimethylsiloxane (PDMS) and rubber, can endow the composite with high stretchability.[15–18] Stretchable composites with high electrical conductivity have been demonstrated;[17] however, limitations are still found in these systems. For example, under high strain the metal nanomaterial-formed conductive framework often breaks due to disconnection of the nanomaterials at joints or spallation of the materials from the surface of elastomers;[12] liquid metal-based composites could also fail under high strain due to the leakage of the liquid metal to form the defective points in the composites.[17]

Ag NWs with a large aspect ratio and high conductivity are a popular choice as a conductive filler.[11,12,19] Much effort has been made to assemble the one-dimensional (1D) NWs into a three-dimensional (3D) hierarchical architecture for desired applications.[20,21] Tang *et al.* reported a low-cost strategy to fabricate ultralightweight aerogel monoliths and conducting

[a]School of Materials, Sun Yat-sen University, Guangzhou 510275, China
[b]Department of Electronic Engineering, The Chinese University of Hong Kong, New Territories, Hong Kong SAR, China. E-mail: nzhao@ee.cuhk.edu.hk; cp.wong@mse.gatech.edu
[c]Department of Biomedical Engineering, University of Kentucky, Lexington, KY 40506-0108, USA
[d]Shenyang National Laboratory for Materials Science, Institute of Metal Research, Chinese Academy of Sciences, Shenyang 110016, China
[e]School of Materials Science and Engineering, Georgia Institute of Technology, Atlanta, Georgia 30332, USA

† Electronic supplementary information (ESI) available: Photograph of emulsion, TEM image of Ag NWs, XRT image of the Ag NW/PDMS composite, change of resistance as a function of strain, fitted parameters and change of the conducting pathway and tunneling distance as a function of strain. See DOI: 10.1039/c9ta11225a

This journal is © The Royal Society of Chemistry 2020

Published on 18 December 2019. Downloaded by Chinese University of Hong Kong on 10/25/2021 4:50:13 PM.

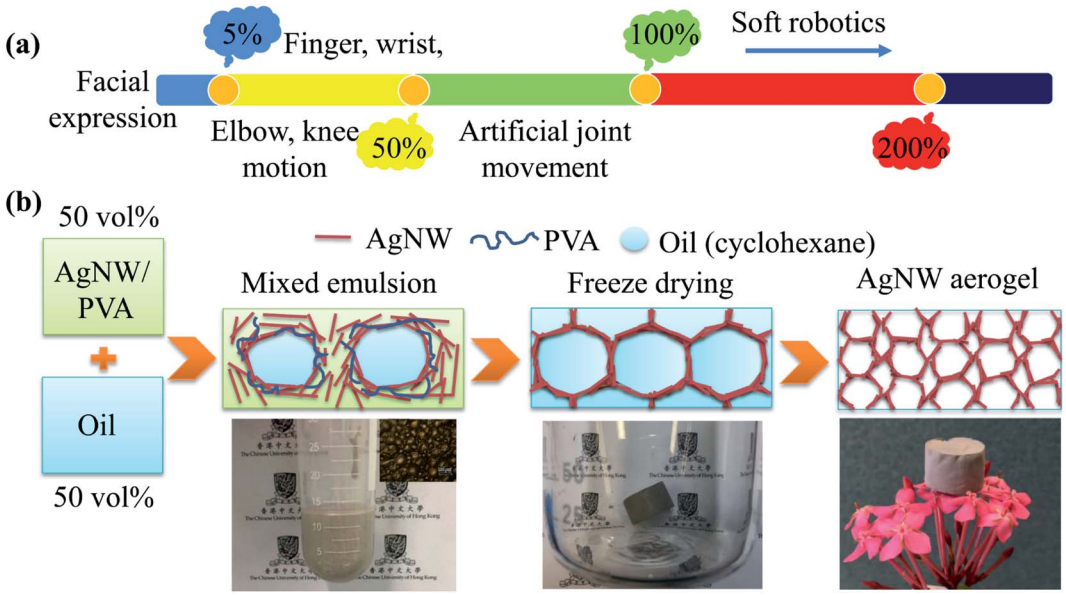

Fig. 1 (a) Illustration of the human body activity and approximate range of strain scales and (b) schematic of the preparation of the Ag NW aerogel. The inset shows the optical image of emulsions.

rubber ambers from copper NWs.[22] In their approach, the Cu NW aerogel was obtained by directly freezing a Cu NW solution; however, the random growth of the ice crystal results in an inhomogeneous distribution of Cu NWs, which may affect the performance reproducibility and reliability of the composite. Oh *et al.* improved the aforementioned method by adding some ice spheres into the Ag NW solution to direct the growth of an isotropic composite structure.[23] Yet, the large size of the ice results in a sparsely distributed Ag NW network and consequently limits the conductivity of the composite. Therefore, alternative template approaches are needed to improve the organization of 1D metallic NWs into a 3D network with a desired microstructure and conductivity for stretchable electronic applications.

In this work, we report an effective and versatile approach to prepare an isotropic and homogenous Ag NW aerogel by an emulsion template method. The Ag NW aerogel displays a hierarchical microstructure with good uniformity and process controllability. To make the aerogel stretchable, we infiltrated the open cells in the aerogel with an elastomer. The obtained composite exhibits a high conductivity and good stretchability at a remarkably low loading density of Ag NWs. A three-dimensional and flexible network is critical for achieving excellent electrical performance at a low percolation threshold.

Experimental

Materials

Ag NWs with a diameter of 20–30 nm and length of 10–20 μm were purchased from Jiangsu XFNANO Materials Tech Co., Ltd. The Ag NWs were washed two times to remove the capping agent by centrifugation. Polyvinyl alcohol (PVA, M_w 85 000–124 000) and cyclohexane were obtained from Sigma-Aldrich. The SYLGARD 184 silicone elastomer base and curing agent were purchased from Dow Corning.

Methods

A concentrated Ag NW solution was prepared by the centrifuging method. No other solvent was used to remove the capping agent. A 5 mL Ag NW solution containing 0.015 g PVA was mixed with equivoluminal cyclohexane and the mixture was shaken by hand acutely for 5 min to get a homogenous emulsion. Then, vacuum degassing was used to remove the bubbles in the emulsion. The emulsion was placed in a sealed plastic container, which was connected with a vacuum pump through a plastic hose. The gas in the emulsion can be removed when the pump is turned on. Ag NW emulsions with different concentrations were poured into a mold and frozen at −40 °C. The shape of the aerogel can be regulated by using different shapes of molds. After 5 h, the frozen samples were taken out of the mold and they were lyophilized by using a Labconco freeze-drier and then the Ag NW aerogel can be achieved. The PDMS prepolymer was made by mixing the base and curing agent in a weight ratio of 15 : 1. The mixture was diluted with cyclohexane and degassed for 10 min. Then, the Ag NW aerogel was formed in a polytetrafluoroethylene mold, following which the PDMS precursor mixture was gently poured into the aerogel filled mold. Degassing was conducted for 5 h to infiltrate the Ag NW aerogel with PDMS followed by thermal curing at 80 °C for 6 h to get the bulk sample.

Characterization

A field-emission scanning electron microscope (SEM, JSM-7800F, JEOL, Japan) was used to characterize the microstructure. The spatial distribution of the Ag NWs and elastomer in the composites was measured using X-ray tomography (XRT,

Published on 18 December 2019. Downloaded by Chinese University of Hong Kong on 10/25/2021 4:50:13 PM.

Versa XRM-500, Xradia, USA). High-resolution transmission electron microscopy was conducted using a Tecnai G2 F20 (FEI, Netherland). The electrical conductivity of the Ag NW/PDMS composites was measured through a four-point probe technique with a Keithley 2400 Source Meter. The stretchability of the Ag NW/PDMS composites was measured using a homemade universal testing machine. The stress distribution of stretching of the Ag NW spheres was simulated with finite element modeling software (COMSOL Multiphysics 5.3a).

Results and discussion

The Ag NW aerogels were obtained through an emulsion-templated assembly process, which is a facile process to generate aerogels with uniform and isotropic microstructures. Fig. 1b shows the schematic diagram of the fabrication process of the Ag NW aerogel. Here an emulsion was applied to construct the porous structure. As water and oil (cyclohexane) are immiscible, oil droplets can be suspended in the water after intense shaking. When Ag NWs are added to the water/oil mixture together with PVA, the NWs can spontaneously distribute around the oil droplets, thus forming a stable emulsion (Fig. S1†). Here, PVA serves as a phase stabilizer and promotes the emulsification process. If no PVA is added, the mixture will transform into two largely separated phases (Fig. S2†) with the oil floating on water due to the Ostwald ripening mechanism.[24] Following the emulsion formation, we applied a freeze drying process to remove the oil and ice to obtain the aerogel. Note that unidirectional freezing with an ice crystal-based template is widely used to form anisotropic architectures.[21,25,26] Our process, on the other hand, exploits spherical oil droplets as a template of pores and would therefore lead to an isotropic microstructure. After the frozen emulsion is lyophilized, a highly porous percolated Ag NW network is formed, with PVA mechanically supporting the Ag NW framework.[22] The inset of Fig. 1b shows that the Ag NW aerogel is very lightweight, which can be supported by petals of a flower. In comparison to the ultralight conductive silver nanowire aerogels developed in a previous study,[26] our Ag NW aerogel possesses an isotropic pore structure and thus has a superior capability of maintaining high conductivity during stretching; furthermore, due to the function of PVA in supporting the Ag NW network, the aerogel also has a higher mechanical strength.

The internal structure of an aerogel plays an important role in the mechanical and electrical properties of the composite. Fig. 2 presents the microstructural images of the as-prepared Ag NW aerogels with different loading densities. It should be noted that the length of the Ag NWs is 10–20 μm and the diameter is 20–30 nm. All the Ag NWs grow along the [1 1 0] direction (Fig. S3†). Fig. 2b, e and h reveal that the pores of the aerogel are spherical and have a diameter of around 100 μm. Also, the pore size increases with increasing concentration of Ag NW. We believe that this size increase is related to the emulsion formation process: when the Ag NW solution and cyclohexane

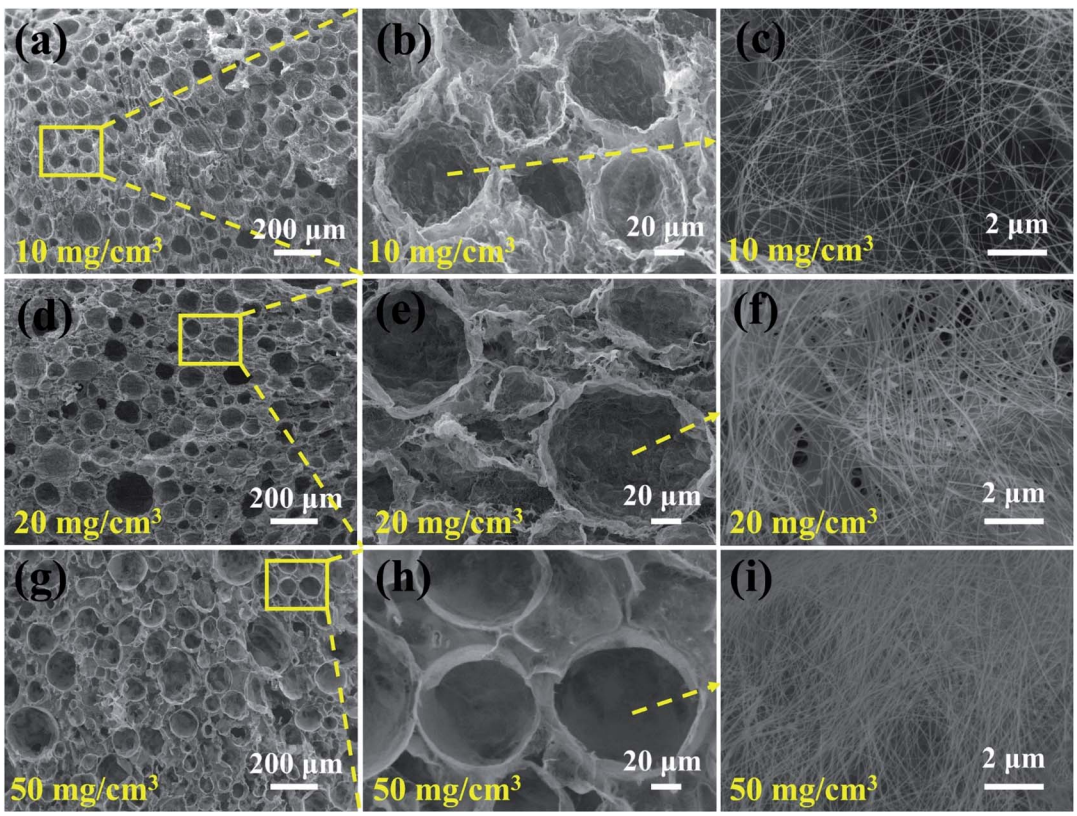

Fig. 2 Microstructures of the Ag NW aerogel with different loading densities: (a–c) 10 mg cm^{-3}, (d–f) 20 mg cm^{-3}, and (g–i) 50 mg cm^{-3}.

 This journal is © The Royal Society of Chemistry 2020

Published on 18 December 2019. Downloaded by Chinese University of Hong Kong on 10/25/2021 4:50:13 PM.

mixture is emulsified under vigorous shaking, the cyclohexane phase is sheared into small droplets under shear force. If the concentration of Ag NWs is increased, the viscosity of the Ag NW solution will be increased accordingly. As a result, the droplet size of cyclohexane will increase, resulting in a larger pore size of the Ag NW aerogel. In addition, the magnified images (*i.e.*, Fig. 2c, f, and i) show that the walls of the pores are formed by randomly intersecting Ag NWs. As the concentration of the Ag NWs increases, the NW network becomes denser, thus generating more conductive pathways. Such hierarchical open-cell structures can allow for full infiltration of an elastomer into the aerogel, as will be discussed later.

To make the aerogel stretchable, we infiltrated the open cells of the aerogel with PDMS (Fig. 3a). The Ag NW aerogel presents good stability and no collapse occurs during the degassing and curing process. No pores are discovered in the sample (Fig. 3b) indicating that the pores in the Ag NW aerogel are open cells. The magnified cross-section image (Fig. 3c) displays a continuous Ag NW conductive pathway and the Ag NW framework is strongly bonded with PDMS without the presence of cracks which can increase the reliability of the composites. We further performed X-ray tomography (XRT) for 3D visualization of the internal microstructure of the composites. Fig. 3d and S4† illustrate the overall XRT images of the Ag NW/PDMS composites, while Fig. 3e and f show the distribution of the Ag NWs and PDMS, respectively. Ag NWs construct an isotropic and hierarchical 3D interconnected structure and PDMS fully infiltrates into the pores. The 3D Ag NW scaffold and PDMS framework contribute to the electronic conductivity and stretchability, respectively. In addition, the uniform distribution of Ag NWs and PDMS ensures the reliability of the performance.

The electrical conductivity of the Ag NW/PDMS composite was measured, and the results are displayed in Fig. 4a. It can be seen that the conductivity of the composite increases almost linearly with the loading of the Ag NWs, with the highest conductivity reaching 65.7 S m^{-1} at a loading density of 50 mg cm^{-3}. The excellent electrical conductivity can be attributed to the efficient and abundant charge transport pathways through the well-interconnected network of highly conductive Ag NWs. We further test the variation of the electrical resistance ($\Delta R = R - R_0$, R and R_0 represent the measured resistance and original resistance of the composites, respectively) of the composites during stretching (Fig. 4b). In general, for all the composites, regardless of their NW loading density, the change of their electrical resistance increases with the amount of tension experienced by the sample. The Ag NW/PDMS composite with a higher Ag NW loading presents a smaller change in its electrical resistance. Fig. S5† shows the magnified image of ΔR as a function of tensile strain of Ag NW/PDMS composites with 50 mg cm^{-3} of Ag NW. It expresses very small changes of resistance and less than 0.7 ohms at 130% strain, which already meets the application requirements of soft electronics in the human body. The result suggests that the unique isotropic microstructure of the Ag NW/PDMS composites is beneficial for maintaining the good conductivity of the material within a wide stretching range.

To further explain the origin of the excellent electrical performance of the Ag NW/PDMS composites under stretching, we performed a simulation of the deformation of a spherical Ag NW architecture under a strain of 30% (Fig. 4c). The result reveals that the Ag NW skeleton will change its shape to accommodate external stress and that the stress will concentrate in the middle of the Ag NW sphere. The changes in the microstructure of Ag NW/PDMS composites were investigated by the *in situ* tension test. As displayed in Fig. 4d–g, the spherical Ag NW framework gradually becomes elliptical with

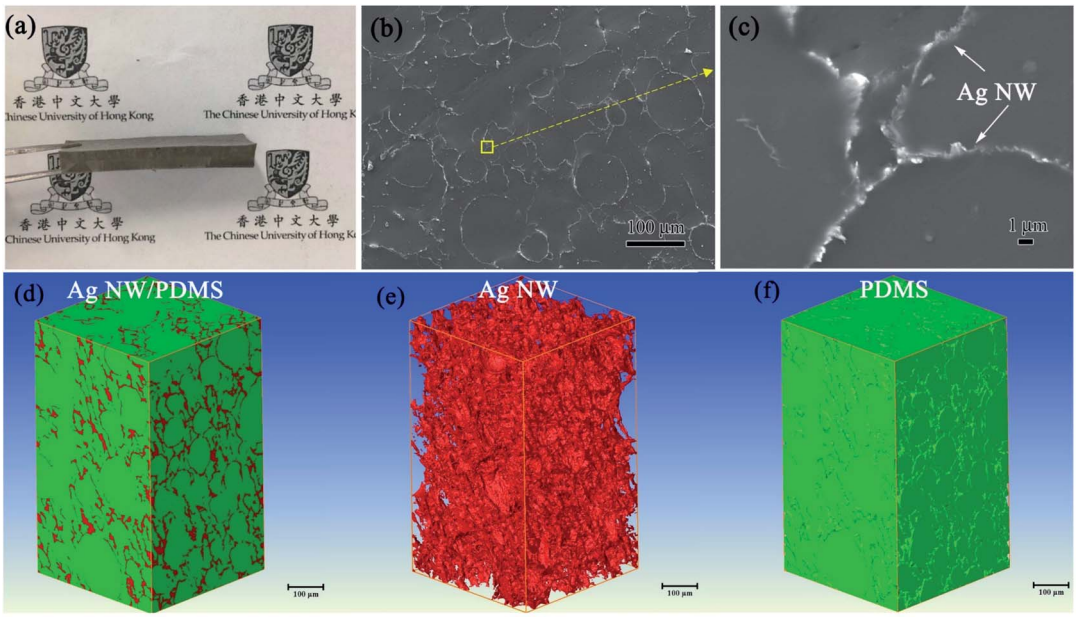

Fig. 3 (a) Optical image, (b) cross-section image and (c) magnified image of the Ag NW/PDMS composite. XRT image of the (d) overall Ag NW/PDMS composite, (e) Ag NW skeleton, and (f) PDMS framework (Ag NW density: 50 mg cm^{-3}).

Published on 18 December 2019. Downloaded by Chinese University of Hong Kong on 10/25/2021 4:50:13 PM.

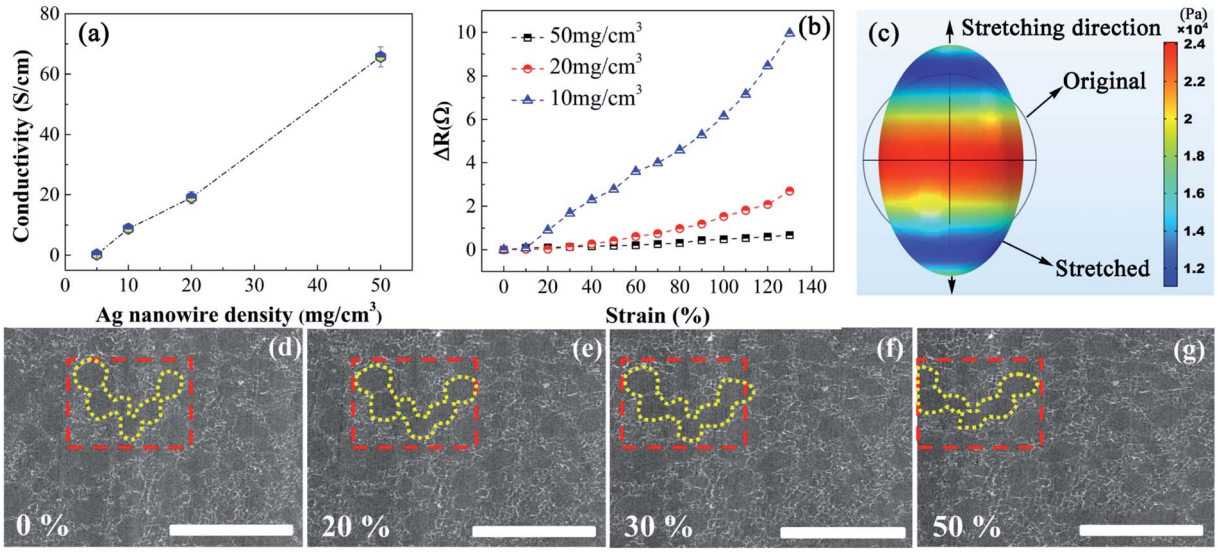

Fig. 4 (a) Electrical conductivity of the Ag NW/PDMS composites at different densities of Ag NWs, (b) change of resistance of Ag NW/PDMS composites as a function of uniaxial tensile strain until fracture, (c) simulation of the stress distribution of the Ag NW skeleton after stretching and (d–g) microstructural images of Ag NW/PDMS composites at 0%, 20%, 30% and 50% tensile strain, respectively (scale bar: 500 μm). The red boxes highlight a sample region as an example to show the deformation of the spherical pores to an elliptical shape during stretching.

the increase of the tensile strain. Such deformation reduces the local strain at the Ag NW-formed walls of the pore structure, as illustrated in Fig. S6,† thus allowing the composite to maintain its conductivity at a high strain value. In this sense, the 3D Ag NW micro-pore structures are generally more desirable for stretchable electronic applications than 2D Ag NW frameworks. We also analysed the variation of the electrical conductivity with different Ag NW densities using the tunneling model proposed by Simmons.[27,28] Based on the model we calculated the change of the conductive pathways and tunneling distance based on the fitting parameters (Table S1†) extracted from the resistivity–strain curves and plotted the results against strain as shown in Fig. S7.† It is found that the number of conducting paths in the Ag NW/PDMS composite with a higher Ag NW density decreases more slowly than that with a lower Ag NW density, and the tunneling distance of the former also increases at a much lower rate, both agreeing well with the experimental observations.

To evaluate the reliability of the composites, we further conduct the cycling test of the Ag NW/PDMS composites at a maximum strain of 50% (Fig. 5a). In the first stretching cycle, the resistance increased by 35% ($\Delta R/R_0 = (R - R_0)/R_0$) at a maximum strain of 50%; after releasing the load, the irreversible resistance increase was only about 18% under 50% stretching. Partial breaking or sliding of Ag NWs mainly

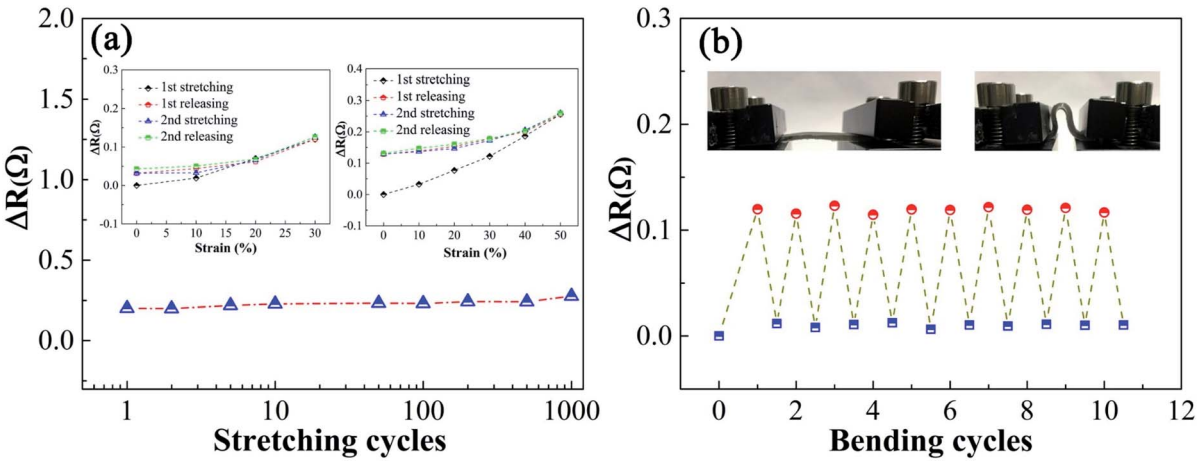

Fig. 5 Resistance change (ΔR) of the Ag NW/PDMS composites under mechanical deformation. (a) ΔR of Ag NW/PDMS as a function of stretching cycles at a strain of 50%. Inset: the ΔR of the composite as a function of tensile strain up to 30% and 50% in the first two stretching–releasing cycles. (b) ΔR of a composite when bent to a radius of 3.0 mm and then released for each cycle. Inset: the composite at a bending radius of up to 3.0 mm in the first bending cycle; photographs show the bending process.

 This journal is © The Royal Society of Chemistry 2020

Published on 18 December 2019. Downloaded by Chinese University of Hong Kong on 10/25/2021 4:50:13 PM.

Table 1 Comparison of conductivity, concentration of filler, and change of electrical resistance ($\Delta R/R_0$) at 100% strain or maximum strain with previously reported systems with a 3D conductive framework

Conducting filler/polymer	$\Delta R/R_0$	Loading (mg cm^{-3})	Conductivity (S cm^{-1})
3D graphene/PDMS[9]	209% at 95% strain	5	10
3D Ag NW/PDMS[21]	67% at 100% strain	60	49.1
Cu NW/PDMS[22]	19.5% at 60% strain	10	0.83
3D Ag NW/PDMS[23]	142% at 100% strain	20	42.36
3D Ag NW/cotton[29]	182% at 100% strain	—	56.82
PUS/Ag NW/PDMS[30]	160% at 100% strain	20	10.25
3D Ag NW/PU[31]	430% at 100% strain	73	20
Graphene/Ag NW/PDMS[32]	250% at 40% strain	18	10.28
Carbon nanotube/PU[33]	52% at 100% strain	64	1
Ag NW/PDMS (this work)	69% at 100% strain	50	65.7

contributes to this phenomenon. When decreasing the tensile strain, the loss of conductivity will also reduce. The Ag NW/PDMS composite shows a stable performance even after 1000 stretching and releasing cycles. The irreversible resistance increase does not enhance after the second cycle. In addition, the bending test was performed at a bending radius of 3 mm. The resistance increases slightly and nearly recovers to the initial state after releasing (Fig. 5b). The stretching and bending tests of the Ag NW/PDMS composites demonstrate their good reliability for application as stretchable conductors.

Finally, it is worth noting that a low NW loading ratio could lead to a lower material cost and better mechanical flexibility of the composite. Therefore, we compare our Ag NW/PDMS composites with previously reported systems with a 3D conductive framework in a comprehensive chart containing base conductivity, filler loading, and change of electrical resistance at 100% or maximum strain (Table 1).[9,21–23,29–33] Ag NW/PDMS prepared using the isotropic aerogel shows a great advantage. It can achieve high conductivity and the low increase of resistance under deformation at a small amount of loading of Ag NW fillers demonstrates its potential application as flexible conductors.

Conclusions

In summary, a 3D porous Ag NW aerogel was developed by an emulsion-template method. 1D short Ag NWs can be efficiently assembled with isotropic and hierarchical architecture. The open cells in the aerogel guarantee that the elastomer fully infiltrates into it and results in a high stretchability. Ag NW/PDMS composites consist of percolation networks of conductive Ag NW fillers in an elastomeric matrix and they can achieve high conductivity at a very low concentration of Ag NWs. Application of the 3D Ag NW scaffold with homogeneous architecture is a cost-effective strategy to realize good performance. The results highlight the Ag NW/PDMS composites as promising stretchable conductors in soft electronics for application in the human body. Furthermore, the emulsion-template method is a versatile strategy for the fabrication of porous aerogels and it can be easily extended to other highly conductive materials (*e.g.* metal nanowires, carbon nanotubes, and graphene) which show advantages in efficiency and uniformity.

Conflicts of interest

There are no conflicts to declare.

Acknowledgements

This work is supported by the Research Grants Council of Hong Kong (GRF No. 14207615).

References

1 S. Han, C. Liu, H. Xu, D. Yao, K. Yan, H. Zheng, H. Chen, X. Gui, S. Chu and C. Liu, *npj Flexible Electron.*, 2018, **2**, 16.
2 S. Choi, S. Han, D. Kim, T. Hyeon and D. Kim, *Chem. Soc. Rev.*, 2019, **48**, 1566.
3 J. Jeong, W. Yeo, A. Akhtar, J. Norton, Y. Kwack, S. Li, S. Jung, Y. Su, W. Lee, J. Xia, H. Cheng, Y. Huang, W. Choi, T. Bretl and J. Rogers, *Adv. Mater.*, 2013, **25**, 6839.
4 T. Cheng, Y. Zhang, W. Lai and W. Huang, *Adv. Mater.*, 2015, **27**, 3349.
5 S. Choi, H. Lee, R. Ghaffari, T. Hyeon and D. Kim, *Adv. Mater.*, 2016, **28**, 4203.
6 S. Yao and Y. Zhu, *Adv. Mater.*, 2015, **27**, 1480.
7 R. Ma, S. Kwon, Q. Zheng, H. Kwon, J. Kim, H. Choi and S. Baik, *Adv. Mater.*, 2012, **24**, 3344.
8 Y. Zhang, C. Sheehan, J. Zhai, G. Zou, H. Luo, J. Xiong, Y. Zhu and Q. Jia, *Adv. Mater.*, 2010, **22**, 3027.
9 Z. Chen, W. Ren, L. Gao, B. Liu, S. Pei and H. Cheng, *Nat. Mater.*, 2011, **10**, 424.
10 Z. Xu, Z. Liu, H. Sun and C. Gao, *Adv. Mater.*, 2013, **25**, 3249.
11 P. Lee, J. Lee, H. Lee, J. Yeo, S. Hong, K. Nam, D. Lee, S. Lee and S. Ko, *Adv. Mater.*, 2012, **24**, 3326.
12 S. Lee, S. Shin, S. Lee, J. Seo, J. Lee, S. Son, H. Cho, H. Algadi, S. Al-Sayari, D. Kim and T. Lee, *Adv. Funct. Mater.*, 2015, **25**, 3114.
13 M. Dickey, *Adv. Mater.*, 2017, **29**, 1606425.
14 C. Li, Q. Li, X. Long, T. Li, J. Zhao, K. Zhang, S. E, J. Zhang, Z. Li and Y. Yao, *ACS Appl. Mater. Interfaces*, 2017, **9**, 29047.
15 S. Wagner and S. Bauer, *MRS Bull.*, 2012, **37**, 207.
16 T. Trung and N. Lee, *Adv. Mater.*, 2017, **29**, 1603167.

Published on 18 December 2019. Downloaded by Chinese University of Hong Kong on 10/25/2021 4:50:13 PM.

17 W. Dang, V. Vinciguerra, L. Lorenzelli and R. Dahiya, *Flexible Printed Electron.*, 2017, **2**, 013003.
18 C. Yua, W. Gong, W. Tian, Q. Zhang, Y. Xu, Z. Lin, M. Hu, X. Fan and Y. Yao, *Compos. Sci. Technol.*, 2018, **160**, 199.
19 C. Jeong, J. Lee, S. Han, J. Ryu, G. Hwang, D. Park, J. Park, S. Lee, M. Byun, S. Ko and K. Lee, *Adv. Mater.*, 2015, **27**, 2866.
20 J. Lee, P. Lee, H. Lee, D. Lee, S. Lee and S. Ko, *Nanoscale*, 2012, **4**, 6408.
21 H. Gao, L. Xu, F. Long, Z. Pan, Y. Du, Y. Lu, J. Ge and S. Yu, *Angew. Chem., Int. Ed.*, 2014, **53**, 4561.
22 Y. Tang, S. Gong, Y. Chen, L. Yap and W. Cheng, *ACS Nano*, 2014, **8**, 5707.
23 J. Oh, D. Lee and S. Hong, *ACS Appl. Mater. Interfaces*, 2018, **10**, 21666.
24 P. Taylor, *Adv. Colloid Interface Sci.*, 1998, **75**, 107.
25 X. Zeng, Y. Yao, Z. Gong, F. Wang, R. Sun, J. Xu and C. Wong, *Small*, 2015, **11**, 6205.
26 F. Qian, P. Lan, M. Freyman, W. Chen, T. Kou, T. Olson, C. Zhu, M. Worsley, E. Duoss, C. Spadaccini, T. Baumann and T. Han, *Nano Lett.*, 2017, **17**, 7171.
27 A. Kim, J. Ahn, H. Hwang, E. Lee and J. Moon, *Nanoscale*, 2017, **9**, 5773.
28 J. Simmons, *J. Appl. Phys.*, 1963, **34**, 1793.
29 C. Zhu, L. Li, J. Wang, Y. Wu and Y. Liu, *RSC Adv.*, 2017, **7**, 51.
30 J. Ge, H. Yao, X. Wang, Y. Ye, J. Wang, Z. Wu, J. Liu, F. Fan, H. Gao, C. Zhang and S. Yu, *Angew. Chem., Int. Ed.*, 2013, **52**, 1654.
31 C. Weng, Z. Dai, G. Wang, L. Liu and Z. Zhang, *ACS Appl. Mater. Interfaces*, 2019, **11**, 6541.
32 C. Wu, L. Fang, X. Huang and P. Jiang, *ACS Appl. Mater. Interfaces*, 2014, **6**, 21026.
33 M. Shin, J. Oh, M. Lima, M. Kozlov, S. Kim and R. Baughman, *Adv. Mater.*, 2010, **22**, 2663.

 This journal is © The Royal Society of Chemistry 2020